JGR Oceans

RESEARCH ARTICLE
10.1029/2019JC015328

Influence of Near-Surface Currents on the Global Dispersal of Marine Microplastic

David Wichmann[1,2], **Philippe Delandmeter**[1], **and Erik van Sebille**[1,2]

[1]Institute for Marine and Atmospheric research Utrecht, Utrecht University, Utrecht, Netherlands, [2]Centre for Complex Systems Studies, Utrecht University, Utrecht, Netherlands

Key Points:
- Submerged microplastic follows significantly different transport routes than at the surface
- No accumulation zones exist at depths below 60 m
- Near-surface currents transport microplastic from subtropical to polar regions

Supporting Information:
- Supporting Information S1

Correspondence to:
D. Wichmann,
d.wichmann@uu.nl

Citation:
Wichmann, D., Delandmeter, P., & van Sebille, E. (2019). Influence of near-surface currents on the global dispersal of marine microplastic. *Journal of Geophysical Research: Oceans*, *124*, 6086–6096. https://doi.org/10.1029/2019JC015328

Received 28 MAY 2019
Accepted 31 JUL 2019
Accepted article online 6 AUG 2019
Published online 23 AUG 2019

Abstract Buoyant microplastic in the ocean can be submerged to deeper layers through biofouling and the consequent loss of buoyancy or by wind-induced turbulent mixing at the ocean surface. Yet the fact that particles in deeper layers are transported by currents that are different from those at the surface has not been explored so far. We compute 10-year trajectories of 1 million virtual particles with the Parcels framework for different particle advection scenarios to investigate the effect of near-surface currents on global particle dispersal. We simulate the global-scale transport of passive microplastic for (i) particles constrained to different depths from the surface to 120-m depth, (ii) particles that are randomly displaced in the vertical with uniform distribution, (iii) particles subject to surface mixing, and (iv) for a 3-D passive advection model. Our results show that the so called "garbage patches" become more "leaky" in deeper layers and completely disappear at about 60-m depth. At the same time, subsurface currents can transport significant amounts of microplastic from subtropical and subpolar regions to polar regions, providing a possible mechanism to explain why plastic is found in these remote areas. Finally, we show that the final distribution in the surface turbulent mixing scenario with particle rise speed $w_r = 0.003$ m/s is very similar to the distribution of plastic at the surface. This demonstrates that it is not necessary to incorporate surface mixing for global long-term simulations, although this might change on more local scales and for particles with lower rise speeds.

1. Introduction

Plastic pollution in the ocean has become one of the major environmental concerns in recent years. Plastic debris has been found in all five ocean basins (Cozar et al., 2014), in the deep sea (Woodall et al., 2014), and has been measured at the poles and in sea ice (Peeken et al., 2018; Obbard et al., 2014; Waller et al., 2017). Debris can be transported thousands of kilometers away from its source by ocean currents and is hence a global environmental problem. Owing to the complexity of the ocean currents, numerical modeling is an essential tool for understanding the transport pathways and accumulation patterns of marine plastic debris (Hardesty et al., 2017).

Transport modeling has proven to be successful in explaining the distribution of surface microplastic. The high concentrations in the subtropical gyres, often called "garbage patches," are mainly a consequence of the converging Ekman component of the surface velocities (Kubota, 1994; Kubota et al., 2005). The fact that many numerical studies find more or less the same surface accumulation pattern irrespective of circulation models, temporal and spatial resolution, and spatiotemporal plastic input scenarios (Eriksen et al., 2014; Lebreton et al., 2012; Maximenko et al., 2012; van Sebille et al., 2012, 2015) indicates a rather strong robustness of surface transport, sharing some similarity with an attractor of a dynamical system: Small perturbations such as differences in the circulation models, subgrid scale effects, and uncertain initial conditions hardly change the long-term distribution of surface debris. Note that the individual garbage patches all play the role of (approximate) attractors (Froyland et al., 2014), such that the kind of robustness described above is only expected within each basin separately. While a strong attractor is a convenient property in modeling transport rates and final distributions in a highly uncertain flow (such as in marine plastic modeling), one may be tempted to overemphasize the role of the surface *flow* based on more or less accurately simulating the spatial *distribution* of surface plastic. A strong attractor at the ocean surface could in principle eliminate some of the history of a particle ensemble. Degradation processes or sinking would then not produce an easily observable signal in the surface distribution. Simulations of the two-dimensional surface

dynamics, though inaccurate on the individual particle level, could still produce accurate results for the distribution in the attractor region.

This is likely to be the case in the ocean due to two facts. First, it is difficult to reconcile the total surface plastic amount estimated with observations and modeling (Cozar et al., 2014; Eriksen et al., 2014; Lebreton et al., 2018; van Sebille et al., 2015) with the estimated amount of plastic available to enter the ocean (Jambeck et al., 2015). Typically, in these studies the observed amounts at the surface are at the order of 1% of the estimated amount entering the ocean in 2010 only (according to Jambeck et al., 2015), whereas around half of the produced plastic is initially buoyant (Barnes et al., 2009). Second, microplastic has been found in regions far off the subtropical accumulation regions such as the Southern Ocean and Antartica (Cincinelli et al., 2017; Isobe et al., 2017; Waller et al., 2017) and in the Arctic (Lusher et al., 2015; Peeken et al., 2018; Obbard et al., 2014). As discussed in these studies, it is often not clear whether microplastic in the polar regions originates from local sources or if there are significant transport pathways from lower latitudes into these regions, and the answer may very well depend on the specific sampling location. If transport pathways from lower, subtropical latitudes exist, however, these can hardly be explained by the strongly converging surface currents, although some of the polar transport can also be explained by wave-induced Stokes drift (Fraser et al., 2018), and perhaps also by atmospheric transport (Allen et al., 2019). These points show that near-surface transport, rather than surface transport, in the water column could play a crucial role in the global dispersion of marine microplastic. In fact, it has been shown that through biofouling, initially buoyant plastic might lose its buoyancy within a few weeks to months (Fazey & Ryan, 2016; Kaiser et al., 2017), which is much less than the typical time scale of attraction of a garbage patch (several years; see Figure S1 in the supporting information). What happens with nonbuoyant microplastic in the water column is however rather poorly understood. Kooi et al. (2017) developed a model for explaining the size-selective behavior of surface plastic removal and showed that particles can in principle stay in the water column, performing oscillations in the vertical caused by subsequent fouling and defouling, as was also described by Ye and Andrady (1991). For such kind of particles, it is obvious that subsurface currents are the ones that govern their motion and not the currents at the surface and the former are expected to differ strongly from the latter due to the exponential decay of Ekman velocities as well as baroclinic pressure gradients. In particular, we expect less pronounced accumulation regions at depth due to the decay of the Ekman velocity.

In addition to biofouling and buoyancy loss, buoyant plastic particles at the ocean surface can be transported to deeper layers through wind-induced turbulent mixing, which leads to an exponentially decreasing depth profile of plastic concentrations depending on the particle rise velocity and local wind conditions (Kukulka & Brunner, 2015; Kukulka et al., 2012; Reisser et al., 2015). This effect was shown to be important when comparing simulation results to measured surface concentrations, as surface trawl nets usually sample the uppermost part of the ocean only. The potential underestimation of the total amount of marine plastic was at first demonstrated by Kukulka et al. (2012), and since then, simulation results and measured concentrations have been corrected for such effects (e.g., Eriksen et al., 2014; Lebreton et al., 2018; van Sebille et al., 2015). In the simulations performed so far, however, the effect of turbulent mixing was considered only after the simulation of trajectories, which does not take into account a potential effect of varying flow fields with depth. Clearly, a weakly buoyant particle will spend, through turbulent mixing, more time deep in the water column than at the surface because once submerged, it needs more time to rise back to the surface.

Lastly, very small plastic particles are expected to behave very similarly to passive water parcels, with only little dependence on particle density. This is intuitively clear by considering Stokes' law for the rise velocity of a suspended particle, which depends linearly on the density difference, but quadratically on the particle diameter (e.g., Batchelor, 2000). Very small particles, even with a lower density than water, are therefore only very weakly buoyant and are likely transported by the full three-dimensional currents, rather than the surface currents.

It should be emphasized that there is a range of other possible processes that can have an effect on plastic transport pathways, and which are not addressed in this paper. To name only a few, particle properties such as composition, size, and shape can have an impact on global transport pathways because they affect the surface removal rate through biofouling (Fazey & Ryan, 2016; Ryan, 2015), on the rise velocity of submerged particles (Kooi et al., 2016; Reisser et al., 2015), and can lead to inertial effects of a particle in a fluid (e.g., Haller & Sapsis, 2008). Shape, size, and buoyancy of a plastic particle can also change in time

due to fragmentation through degradation (Cole et al., 2011). The beaching of plastic particles, for example, through breaking waves is far from being understood and could constitute a large sink of plastic. More realistic plastic source scenarios, such as the one of Lebreton et al. (2017), can clearly have an effect on plastic distributions. Oceanographic phenomena such as downwelling and tides may also have a local effect on the transport pathways of plastic particles. All of these processes come with relevant temporal and spatial scales of importance, and it is currently not known to what extent the different processes are important for the global long-term fate and distribution of marine plastic. The large number of uncertainties makes it challenging to model the global dispersion of realistic marine debris. More experimental and numerical efforts are needed to constrain the parameter space that governs the dispersion of marine plastic debris, together with extended measurement campaigns of marine plastic that not only contain plastic counts but also size, composition, and other parameters such as the amount of biofouling.

Here, we do not intend to fully model the realistic dispersion of plastic in the ocean. Neither do we parameterize relevant processes such as degradation nor do we use realistic plastic input scenarios. We rather aim to assess the importance of subsurface advection for the global accumulation and transport pathways of marine debris. Despite the evidence for the importance of vertical transport of microplastic presented above, to our knowledge no study so far has addressed the question how the global accumulation pattern and pathways of microplastic could be influenced by the transport through subsurface instead of surface currents. Yet the importance of measuring plastic throughout the entire water column is starting to get recognized in the plastic community, and our understanding of the dispersal, accumulation, and quantity of plastic might change substantially when deeper measurements become available (Choy et al., 2019). With this paper, we wish to contribute to the understanding of the dynamics of submerged particles, which will also help with the interpretation of deep measurements.

Here, we study this effect through numerically simulating the trajectories of approximately 1 million particles in the global ocean for 10 years of advection for different simulation scenarios. We test the importance of biofouling-related subsurface transport through constraining particles to certain fixed depths and through randomly displacing them in the upper ocean. These models are highly idealized, but due to the lack of precise understanding of the vertical transport dynamics, this can be seen as a first step in studying the consequences of subsurface transport on the global dispersion of marine microplastic. We also study the effect of turbulent surface mixing through explicitly including wind-dependent vertical mixing as a random process, with vertical probability distribution according to Kukulka et al. (2012) in the particle trajectory integration. Finally, we run a simulation where particles are subject to the full three-dimensional currents of our data set.

2. Methods

We simulate the transport of microplastic through modeling the trajectories of Lagrangian particles. We use Version 1.11 of the Parcels framework (oceanparcels.org; Lange & van Sebille, 2017) for the 2-D simulations and Version 2.0 for the 3-D simulation (Delandmeter & van Sebille, 2019). We use current and wind stress data for the 10 years of 2000–2009 from a NEMO ORCA-N006 run, a standard run of NEMO (Madec, 2008), forced by the Drakkar forcing (Dussin et al., 2016; available at http://opendap4gws.jasmin.ac.uk/thredds/nemo/root/catalog.html). The flow and wind stress fields are available on an ORCA grid (Madec & Imbard, 1996) with a 1/12° resolution, provided for every 5 days. The model has 75 vertical levels with an increasing spacing between them for larger depths, 26 of which are within the upper 120 m of the water column.

The fields are interpolated in space and time to the particle position and time with the C-grid interpolation scheme described in Delandmeter and van Sebille (2019). We use the fourth-order Runge-Kutta method with a time step of 10 min for the trajectory integration. For each of the different simulation scenarios (see Table 1), we study the long-term distribution of marine plastic and the transport pathways between different ocean regions (shown in Figure S2) with approximately 1 million particle trajectories starting from a uniform distribution on the vertices of a $0.2^\circ \times 0.2^\circ$ grid on 5 January 2000 and advecting them for 10 years.

We perform runs for four kinds of passive particles: (i) particles constrained to different depths; (ii) particles randomly displaced in the vertical according to a uniform distribution at each time step; (iii) particles that are, again at each time step, randomly displaced in the vertical according to the exponential distribution suggested by Kukulka et al. (2012); and (iv) particles that follow the full three-dimensional flow. (i) also includes a surface run ($z = 0$ m), which serves as a baseline to compare the other simulations to. Simulations

Table 1
Simulation Overview

Simulation	Parameters
(i) Fixed depth	$z = 0, 2, 5, 9, 16, 26, 41, 61, 87, 97, 120$ m[a]
(ii) Uniform mixing	$p(z) = U(0\text{ m}, 120\text{ m})$[b]
(iii) Exponential mixing	$p(z) = \lambda e^{-\lambda z}$, $w_r = 0.003$ m/s, $z < 120$ m[c]
(iv) Full 3-D advection	Initial depth = 1.5 m

[a]The values correspond to the depths within different layers of the hydrodynamic data. [b]Random uniform distribution between top layer at $z = 0$ m and $z = 120$ m. [c] See the text for the definition of λ.

with particle constrained to certain depths (i) represent the horizontal advection of particles in the water column. The assumption of a fixed depth is a strong simplification, but it allows us to gain first insights into the transport of submerged plastic particles with a reasonable computational cost and with no additional assumptions on real vertical transport mechanisms. Similarly, the simulation of the uniformly displaced particles serves as a simple model where particles can move to any other position in the upper water column, either due to biofouling or wind-induced mixing with very low buoyancy. Simulations (i)–(iii) neglect vertical flow velocities and are confined to the depth interval [0 m, 120 m]. One-hundred-twenty meters is the depth where the concentration for very weakly buoyant particles with rise speed $w_r = 0.003$ m/s under strong wind conditions of $\tau = 0.8$ Pa decreases to roughly 20% of the surface concentration within the parameterization of Kukulka et al., 2012 (2012; see below), such that it captures the largest part of the turbulent mixing range in the surface layer. It also comprises the range of depths within which biofouled initially buoyant microplastic particles oscillate in the water column according to the model of Kooi et al. (2017; which ranges typically to around 60 m; see their Figure S1). The simulation of passive particles at the surface (at $z = 0$ m) is similar to the approach of most previous studies on surface microplastic (e.g., Eriksen et al., 2014; Lebreton et al., 2012; van Sebille et al., 2015). For the 3-D simulation (iv), we place the particles at an initial depth just below the surface at $z = 1.5$ m as we work with a nonmoving ocean surface such that the vertical velocity is set to zero at $z = 0$ m by definition. This is similar to the methodology in Delandmeter and van Sebille (2019).

According to Kukulka et al. (2012), the depth-dependent plastic concentration $n(z)$ follows an exponential distribution (we take the z axis pointing downward):

$$n(z) \propto \exp(-\lambda z). \tag{1}$$

Here $\lambda = w_r/A_0$, where w_r is the rise velocity of the buoyant particle and $A_0 = 1.5 u_{*w} \kappa H_s$ with u_{*w} the frictional velocity of water, $\kappa = 0.4$ the van Karman constant, $H_s = 0.96 g^{-1} \sigma^{3/2} u_{*a}^2$ with gravitational constant g, wave age σ, and frictional air velocity u_{*a}. As in Kukulka et al. (2012), we take $\sigma = 35$. The frictional velocities of air and water are determined by the wind conditions, given by $u_{*w} = \sqrt{\frac{|\vec{\tau}|}{\rho_w}}$ for water with wind stress $\vec{\tau}$ and water density ρ_w. Finally, the frictional velocity of air is defined by $u_{*a} = \sqrt{\frac{|\vec{\tau}|}{\rho_a}}$. Taking $\rho_w = 1{,}027$ kg/m^3 and $\rho_a = 1.22$ kg/m^3 leads to $A_0 = 0.31 \cdot |\vec{\tau}|^{3/2}$, where $|\vec{\tau}|$ is given in pascals and A_0 in square meters per second. We model turbulent mixing through randomly displacing the virtual particles at each time step along the vertical with an exponential probability distribution $p(z) = \lambda e^{-\lambda z}$, where λ depends on the wind stress that is taken from the NEMO data set. This approach assumes that the time scale of turbulent mixing is much faster than the one of particle advection, which is a reasonable assumption. We take a small value of the rise velocity of $w_r = 0.003$ m/s, which is at the lower end of the rise velocities reported by Reisser et al. (2015) and hence simulates an extreme case of strong mixing effects. Table 1 shows the different simulation scenarios of this study (1 million particle trajectories each). The code for the simulations and data analysis is available on GitHub (https://github.com/OceanParcels/near_surface_microplastic).

3. Results

3.1. Particle Distributions

Figure 1 shows the resulting long-term distribution of the surface ($z = 0$ m) particles at the end of the simulation. The accumulation regions in all five subtropical gyres are clearly visible and agree roughly with the expected locations from measured data (compare to, e.g., Figure 1 of van Sebille et al., 2015). Note that many

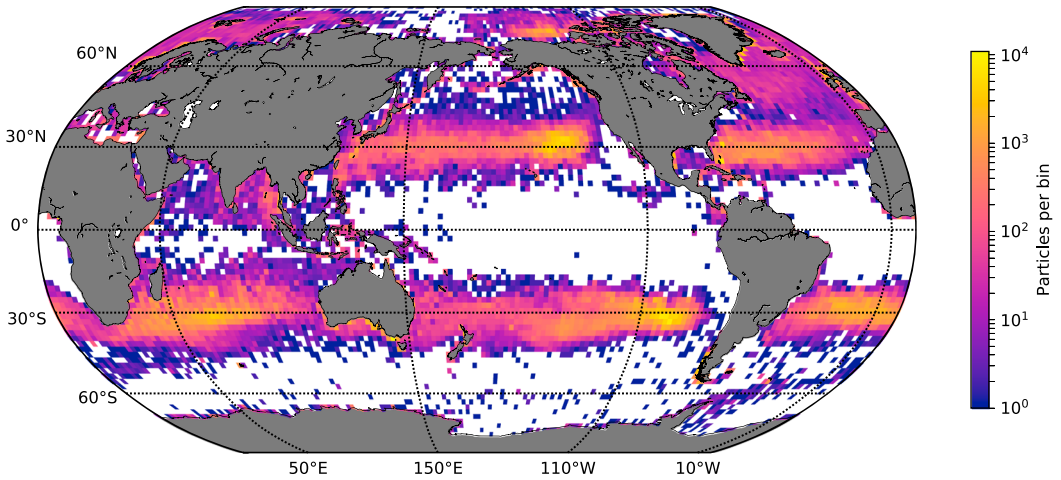

Figure 1. Modeled distribution for surface particles (fixed depth of $z = 0$ m), in logarithmic scale with square binning of 2°. As described in the text, the particles were released uniformly and advected for 10 years.

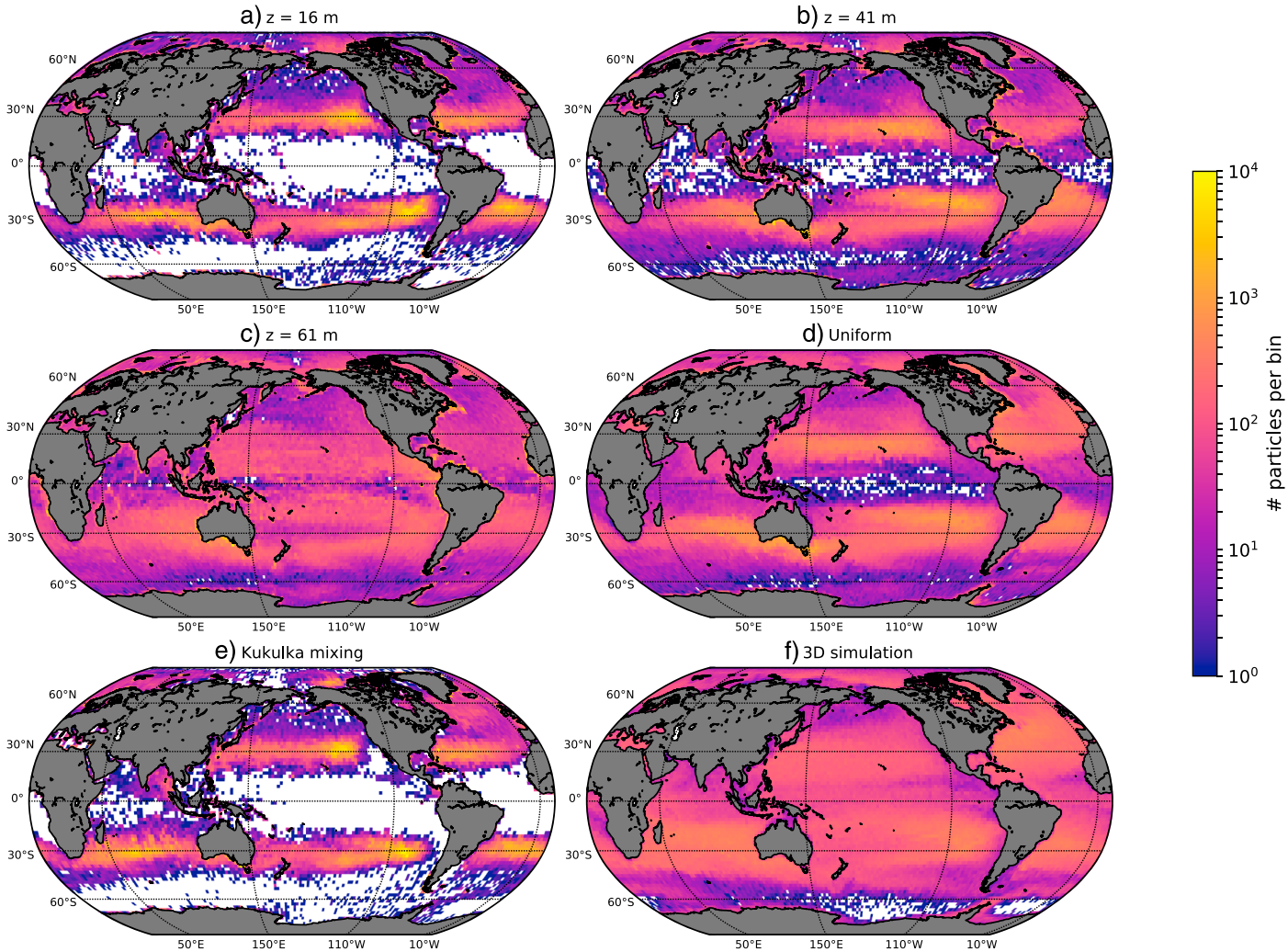

Figure 2. Final distributions of a selection of simulations. The color bars show the number of particles per bin on a square binning of 2°. (a)–(c) show a selection of cases for the fixed-depth simulations (i); see Table 1. (d)–(f) show the results for the other cases (ii–iv). In (d)–(f), the distributions are depth-integrated sums. Similar figures for the other scenarios can be found in Figure S3.

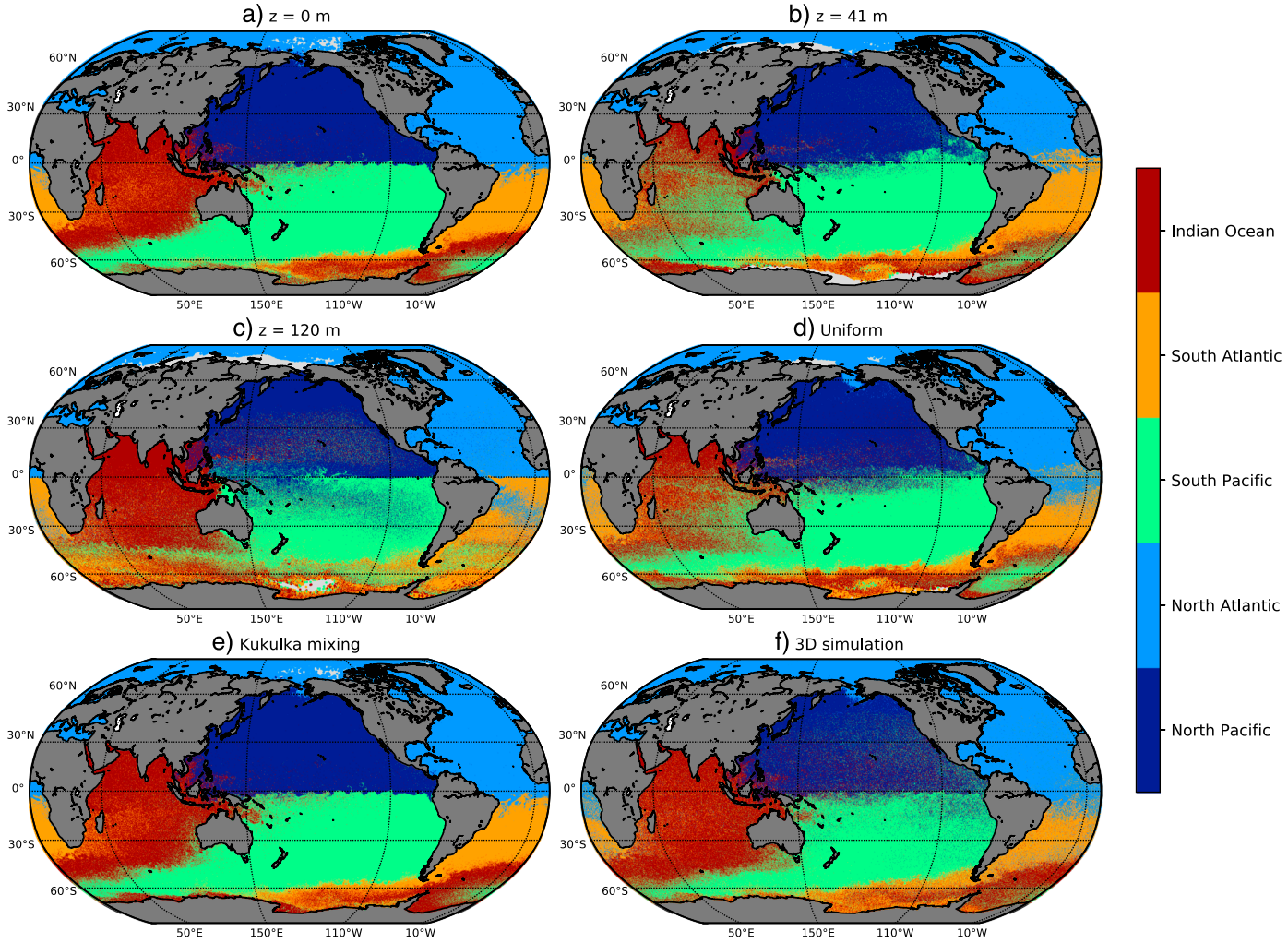

Figure 3. Scatter plot of the initial position of the particles that end up in one of the subtropical basins (indicated by the colors) for a selection of the performed simulations. (a)–(c) show a selection of cases for the fixed-depth simulations (i); see Table 1. (d)–(f) show the results for the other cases (ii–iv). Similar figures for the other scenarios can be found in Figure S4.

regions outside of the gyres are completely depleted of particles after the 10 years of simulation. This distribution did not change significantly in the last few simulated years, indicating that the particle distribution is in an almost-equilibrium state (see Figure S1).

Figure 2 shows the final distribution for a selection of the different scenarios (see Figure S3 for the corresponding maps for the other scenarios), which we compare to the distribution of the surface simulation shown in Figure 1. Note that for Figures 2d–2f, the distributions are shown as depth-integrated sums, that is, distributions of the particles' longitudes and latitudes only. As expected, the strong converging property of the surface flow weakens at depth; see Figures 1 and 2a–2c. The garbage patch structure is still clearly visible in the top part of the water column, with a transition toward more smeared out distributions at 41 m. Note that $z = 16$ m shown in Figure 2a is close to the depth sampled by drogued drifters (Niiler & Paduan, 1995). At 61 m (Figure 2c), no garbage patches exist any more, and the distribution remains essentially unchanged up to the deepest layer considered at $z = 120$ m. Different from the surface flow, the polar and equatorial regions are not as strongly depleted of particles at larger depth any more. This is also the case for the random uniform simulation (Figure 2d), although the patches are still clearly visible. The exponential mixing simulation according to Kukulka et al. (2012) does not show a significant visible difference to the surface simulation on the global scale, as seen in Figure 2e. It should be noted however that this could be an effect of the choice of the rise speed (here $w_r = 0.003$ m/s), which depends on particle composition and size. Smaller particles with even smaller rise speeds would be mixed into deeper layers, and consequently,

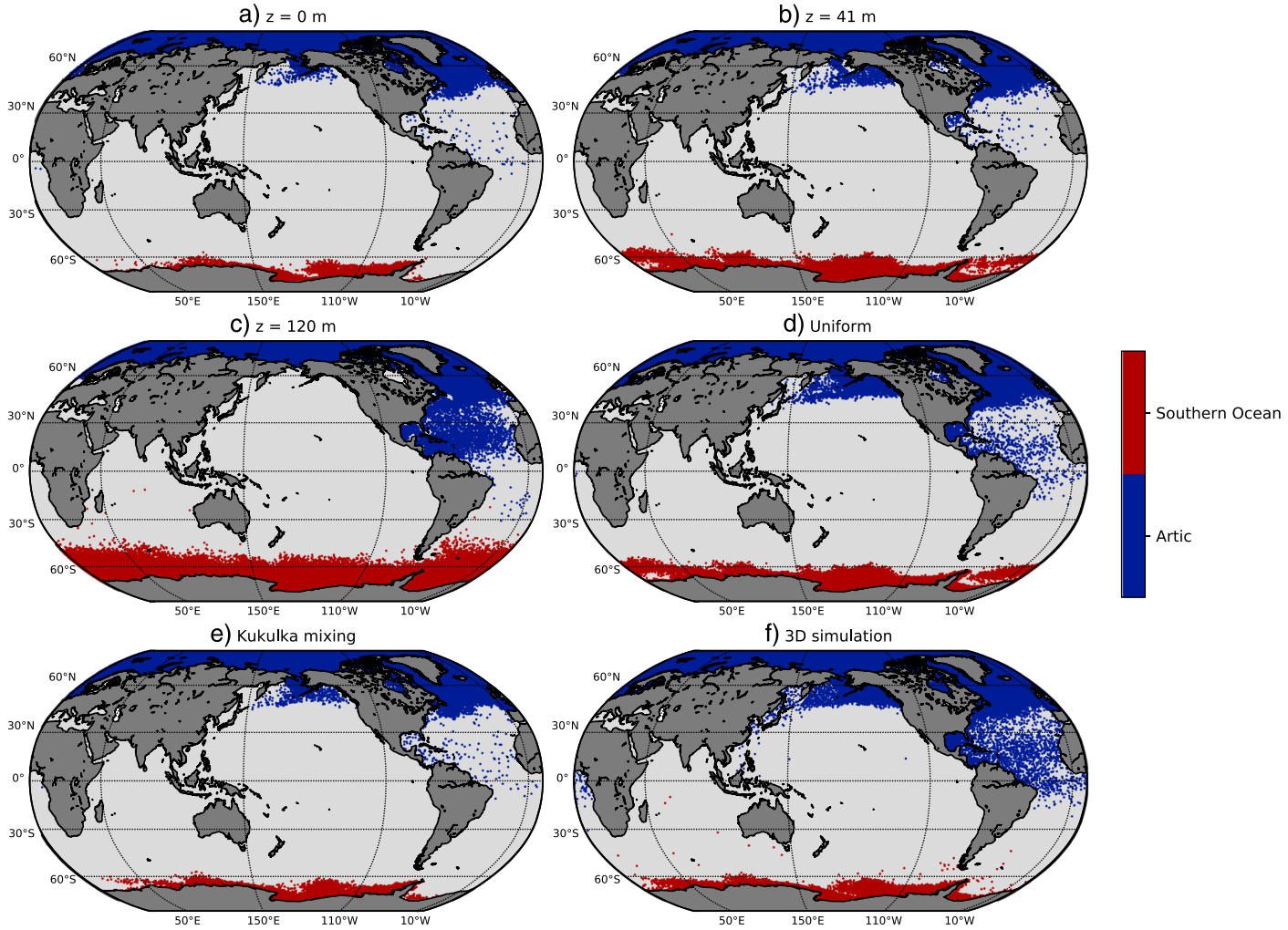

Figure 4. Scatter plot of the initial position of the particles that end up in the polar regions (indicated by the colors) for a selection of the performed simulations. (a)–(c) show a selection of cases for the fixed-depth simulations (i); see Table 1. (d)–(f) show the results for the other cases (ii–iv). Similar figures for the other scenarios can be found in Figure S5.

the effects of turbulent surface mixing would increase. In addition, turbulent mixing could still be important on smaller spatial and temporal scales. The distribution of the 3-D simulation (Figure 2f) does show only very little spatial variation, together with a removal of particles from the Southern Ocean region. Note here that this can also be an effect of our choice of initial condition for the 3-D simulation, as we position the particles close to the surface at a depth of 1.5 m. More than 80% of the particles are still within the upper 350 m of the water column at the end of the simulation (see Figure S6).

3.2. Regional Transport

We next analyze the interregional transport by dividing the ocean into seven regions: North Pacific, North Atlantic, South Pacific, South Atlantic, Indian Ocean, Arctic, and Southern Ocean. A map of the division is shown in Figure S2. The Arctic region is chosen to be north of 65° N latitude and the Southern Ocean to be south of 60° S. We analyze the regions of attraction of the different garbage patches and the connectivity between the polar and lower-latitude regions for the different simulations. Figures 3 and 4 show the final destination plotted in the respective color at the initial location of the particles for those ending up in one of the five subtropical basins and the two polar regions, respectively. In Figure 3a, we see rather well-defined boundaries between the different colors for the surface simulation, as expected. The area of each color here corresponds to the region of attraction of the garbage patches. It is clearly visible that surface particles hardly cross the equator in the Pacific and Atlantic basins. For larger depths (Figures 3b and 3c), however, these borders become smeared out, in particular the border between the Atlantic and Pacific basins, respectively:

There are no clear-cut boundaries between the different basins any more, already at the relatively shallow depths we consider here. Similar plots for the other scenarios are shown in Figure S4. Figures 3a–3c also show that the Indian Ocean plays a somewhat special role, as it becomes more leaky at intermediate depths of $z = 41$ m, and less leaky again for deeper particles at $z = 120$ m. This is different from the other four subtropical basins, which become more leaky monotonously with depth. The result for the uniform mixing scenario in Figure 3d resembles in its broad features the simulation at a depth of $z = 41$ m (Figure 3b). It is again notable that there is no significant visible difference between the surface (Figure 3a) and exponential mixing (Figure 3e) scenarios, although we would expect this to change for smaller rise speeds, as discussed above. Finally, we see in Figure 3f that in the 3-D simulation, the boundaries between the basins are also less clearly defined, in particular for the Atlantic basin. This is expected due to the transport of shallow water from the South to the North Atlantic where deep water is formed (see Figure S6) as part of the thermohaline circulation.

In Figures 4a–4c, we can see that transport toward the poles increases with increasing depth. We also see that the polar North Atlantic is quite well connected to the subtropical North Atlantic already for the surface flow, as was also observed to be the case for surface drifters (Brambilla & Talley, 2006), although this connection increases for larger depths. For the Southern Ocean, at $z = 120$ m particles can originate from parts of the Indian Ocean and from the South Pacific and South Atlantic on the 10-year time scale considered here. This is very different from the surface flow and the 3-D flow, where almost nothing enters the Southern Ocean from the other basins. The effect of the Antarctic Circumpolar Current to prevent transported matter from entering the Southern Ocean hence weakens significantly with depth. Figure 4d shows that the uniform mixing simulation leads to a stronger flow of particles from the northern North Pacific to the Arctic region, compared to the simulations at fixed depths. This is surprising, but it highlights that vertical dynamics can actually matter and that the dynamics of the random uniform simulation is not simply an average of the fixed-depth simulations. As can be seen in Figure 4e, the exponential mixing simulation does again not show significant differences to the surface simulation. Finally, we note that there is also significant inflow from the northern basins into the Arctic region in the 3-D simulation (Figure 4f), as expected from the circulation in the global thermohaline circulation. Note that the fact that there are almost no particles that reach the Southern Ocean regions in the 3-D simulation is again likely to be a consequence of our choice of initial depth of 1.5 m for the particles. Simulation results for the other scenarios are provided in the supporting information (Figure S5).

With Figures 3 and 4 one has to take into account that our simulation is of course limited by an unrealistically low number of particles released only once into the ocean with a uniform distribution. Continuous, spatially heterogeneous release of many more particles, as in the real world, would also lead to different transport into these regions.

Based on the regional division (Figure S2), we form a transport matrix F: If n_{ij} is the number of particles that starts in region i and ends up in region j after 10 years, we define this matrix as $F_{ij} = n_{ij}/\sum_j n_{ij}$, that is, the row normalized form of n_{ij}. The matrix F_{ij} describes the share of those particles that are transported from region i to j compared to all particles that start in region i, and its entries therefore indicate the strength of the particle transport between the different regions. The transfer matrices for all simulations are shown in Tables S1–S14. The main observation is that, apart from the Indian Ocean, the diagonal elements F_{ii} for i a subtropical basin decrease significantly for larger depths, by roughly 7–13% from the surface to $z = 120$ m, demonstrating that the garbage patches in these four basins become less stable in the deep or that their basins of attraction shrink. An exception is the Indian Ocean, whose diagonal element increases by about 10%. Note that these percentages are all sensitive to the choice of basins, which is especially difficult at the boundary between South Pacific and Indian Ocean. The diagonal elements for i = polar region increase by 12% (Arctic) and 60% (Southern Ocean) between the surface and 120 m, showing that particles in these regions are more likely to stay there at larger depth than at the surface.

Figure 5 shows the significant nondiagonal (a and c) and diagonal (b and d) entries of F for transport toward the two polar regions. To assess the robustness under different choices of regional divisions, we computed the transport matrix for different definitions of the Southern Ocean boundary (56°, 60°, 62° S) and the Atlantic-Artic boundary (60°, 65°, 70° N), illustrated by the light-colored areas (for different depths) and error bars (for the other scenarios) in the figure. For the Southern Ocean, we can see that there is no particle transport from the subtropical basins at the surface, but this increases to roughly 7% (South Atlantic),

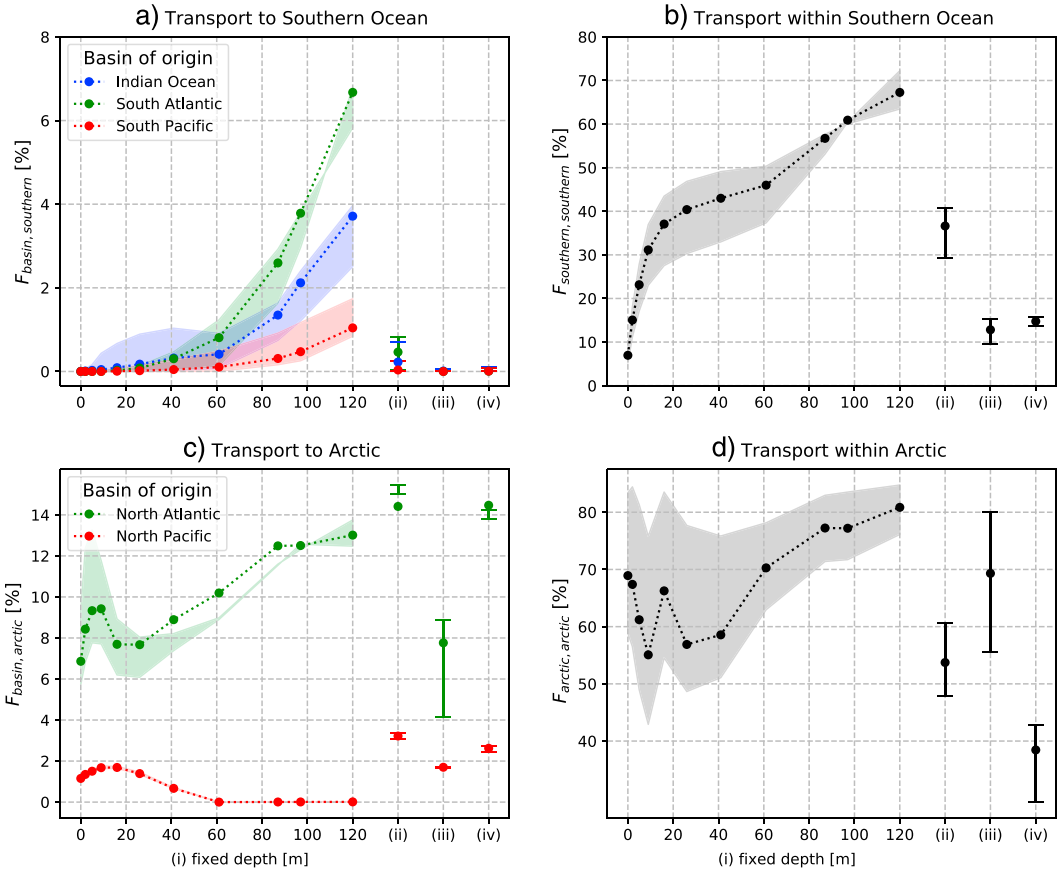

Figure 5. Matrix elements for particle transport to the poles for the different scenarios: fixed depth (i), uniform mixing (ii), exponential mixing (iii), and the 3-D simulations (iv). Note that the plots have different *y* axes. The edges of the light-colored areas (for fixed depths) and error bars (ii–iv) in the figures display the result under different definitions of the Southern Ocean (a and b) boundary (56°, 60°, 62° S) and the Atlantic-Artic (c and d) boundary (60°, 65°, 70° N). The solid markers correspond to the boundaries at 60° S and 65° N, respectively. Note that changing the region boundaries does not affect the transport rates monotonously, such that the rates for different region definitions can intersect, as is particularly visible for the North Atlantic in (c).

4% (Indian Ocean), and 1% (South Pacific). In addition to the stronger import of particles into the Southern Ocean, there is also a weaker export of particles from the Southern Ocean, as can be seen by the strongly increasing diagonal element of F (Figure 5b). The situation is slightly less clear for the Arctic, where transport from the North Atlantic increases with depth, but transport from the North Pacific decreases (Figure 5c). As mentioned earlier, it is especially remarkable here that the random uniform simulation leads to significantly stronger transport from the North Pacific as any of the fixed-depth simulations. Finally, Figure 5d shows that over the whole range of depths the export of particles from the Arctic also seems to decrease (as the diagonal element increases), but this trend is not as significant as for the Southern Ocean. It is visible that the transport rates of the exponential mixing scenario are again very similar to the $z = 0$ m case. It should be noted that there is no monotonous trend between the transport rates and the choice of boundaries of the two polar regions, as is especially visible for the North Atlantic-Arctic transport shown in green color in Figure 5c.

4. Conclusion

The long-term dynamics of surface microplastic is governed by strong basin-scale attracting regions, the garbage patches. Due to their robustness to different simulation scenarios and their ability to explain measured surface concentrations, surface simulations have dominated the recent efforts of global oceanic microplastic modeling. Nevertheless, if transport from subtropical to polar regions exists, this cannot be explained by considering the surface layer only, at least if no additional effects such as wave-induced Stokes

drift (Fraser et al., 2018) or atmospheric transport are taken into account. We provide another possible mechanism to explain such poleward transport: the advection by near-surface currents.

In this study, we tested the potential role of subsurface currents through simulating Lagrangian particle trajectories for 10 years. We performed runs for four kinds of passive particles: (i) particles constrained to different depths; (ii) particles randomly displaced in the vertical according to a uniform distribution at each time step; (iii) particles that are, again at each time step, vertically displaced according to the exponential distribution suggested by Kukulka et al. (2012); and (iv) particles that follow the full three-dimensional flow. The results show that the transport of submerged microplastic is determined by completely different dynamics than at the surface. The decay of the Ekman component with depth not only leads to less convergence and hence less pronounced accumulation spots of plastic but there is also stronger transport from the subtropical and subpolar regions into the polar regions for particles at larger depth. This means that plastic particles in regions of lower latitudes that loose their buoyancy can in principle be transported to originally noncontaminated polar regions. The exponential mixing scenario according to Kukulka et al. (2012) did not show any visible significant difference to the surface simulation, although this would clearly change for particles with smaller rise speeds, which have a higher probability to stay away from the surface for longer times, and potentially also on smaller temporal and spatial scales. The 3-D simulation also showed significant transport into the Arctic, which is a possible mechanism to explain the transport of neutrally buoyant (very small) plastic particles into that region.

We studied the effects of subsurface currents through constraining particles to certain depths, randomly displacing them or advecting them passively with the 3-D flow, all of which are strong simplifications of the real world processes. In addition, our analysis is based on simplified initial conditions of globally uniform particles at one point in time, which affects transport rates between different regions. A full model of realistic plastic particles would need to take into account a range of processes through parameterizations. For example, in the model of Kooi et al. (2017), most particles do not stay at a fixed depth but constantly oscillate in the water column. A more realistic approach to study the effect of biofouling would hence have to couple the Lagrangian advection scheme to a model for the vertical transport of particles, such as the one of Kooi et al. (2017). However, considering the fact that the mechanisms of vertical transport are still not fully understood, this study gives a first indication to the full complexity of marine plastic transport and provides a simple and plausible mechanism to explain how plastic could be transported from subtropical to polar regions. Our results show that there is a need for a better understanding of the sinking processes of plastic and to incorporate such effects in three-dimensional transport modeling in order to close the global marine plastic budget. This is crucial to understand the impact plastic debris can have on remote but through subsurface currents connected pristine ecosystems.

Acknowledgments
David Wichmann, Philippe Delandmeter, and Erik van Sebille are supported through funding from the European Research Council (ERC) under the European Union Horizon 2020 Research and Innovation Programme (Grant 715386). This work was carried out on the Dutch National e-Infrastructure with the support of SURF Cooperative (Project 16371). We thank Andrew Coward for providing the ORCA-N006 simulation data (also available at http://opendap4gws.jasmin.ac.uk/thredds/nemo/root/catalog.html). Some of the ideas in this work benefited from discussions in Scientific Committee on Oceanic Research (SCOR) Working Group 153, which is supported by national committees of SCOR and by Grant OCE-1546580 to SCOR from the U.S. National Science Foundation.

References

Allen, S., Allen, D., Phoenix, V. R., Le Roux, G., Durántez Jiménez, P., Simonneau, A., et al. (2019). Atmospheric transport and deposition of microplastics in a remote mountain catchment. *Nature Geoscience*, *12*(5), 339–344. https://doi.org/10.1038/s41561-019-0335-5

Barnes, D. K. A., Galgani, F., Thompson, R. C., & Barlaz, M. (2009). Accumulation and fragmentation of plastic debris in global environments. *Philosophical Transactions of the Royal Society B: Biological Sciences*, *364*(1526), 1985–1998. https://doi.org/10.1098/rstb.2008.0205

Batchelor, G. K. (2000). *An Introduction to Fluid Dynamics*, (Cambridge Mathematical Library). Cambridge: Cambridge University Press. https://doi.org/10.1017/CBO9780511800955

Brambilla, E., & Talley, L. D. (2006). Surface drifter exchange between the North Atlantic subtropical and subpolar gyres. *Journal of Geophysical Research*, *111*, C07026. https://doi.org/10.1029/2005JC003146

Choy, C. A., Robison, B. H., Gagne, T. O., Erwin, B., Firl, E., Halden, R. U., et al. (2019). The vertical distribution and biological transport of marine microplastics across the epipelagic and mesopelagic water column. *Scientific Reports*, *9*(1), 7843. https://doi.org/10.1038/s41598-019-44117-2

Cincinelli, A., Scopetani, C., Chelazzi, D., Lombardini, E., Martellini, T., Katsoyiannis, A., et al. (2017). Microplastic in the surface waters of the Ross Sea (Antarctica): Occurrence, distribution and characterization by FTIR. *Chemosphere*, *175*, 391–400. https://doi.org/10.1016/j.chemosphere.2017.02.024

Cole, M., Lindeque, P., Halsband, C., & Galloway, T. S. (2011). Microplastics as contaminants in the marine environment: A review. *Marine Pollution Bulletin*, *62*(12), 2588–2597. https://doi.org/10.1016/j.marpolbul.2011.09.025

Cozar, A., Echevarria, F., Gonzalez-Gordillo, J. I., Irigoien, X., Ubeda, B., Hernandez-Leon, S., et al. (2014). Plastic debris in the open ocean. *Proceedings of the National Academy of Sciences*, *111*(28), 10,239–10,244. https://doi.org/10.1073/pnas.1314705111

Delandmeter, P., & van Sebille, E. (2019). The Parcels v2.0 Lagrangian framework: New field interpolation schemes. *Geoscientific Model Development*, *12*. https://doi.org/10.5194/gmd-2018-339

Dussin, R., Barnier, B., Brodeau, L., & Molines, J. M. (2016). The making of Drakkar forcing set DFS5. DRAKKAR/MyOcean Report 01-04-16, LGGE, Grenoble, France.

Eriksen, M., Lebreton, L. C. M., Carson, H. S., Thiel, M., Moore, C. J., Borerro, J. C., et al. (2014). Plastic pollution in the world's oceans: More than 5 trillion plastic pieces weighing over 250,000 tons afloat at sea. *PLoS ONE*, *9*(12), e111913. https://doi.org/10.1371/journal.pone.0111913

Fazey, F. M. C., & Ryan, P. G. (2016). Biofouling on buoyant marine plastics: An experimental study into the effect of size on surface longevity. *Environmental Pollution*, *210*, 354–360. https://doi.org/10.1016/j.envpol.2016.01.026

Fraser, C. I., Morrison, A. K., Hogg, A. M. C., Macaya, E. C., van Sebille, E., Ryan, P. G., et al. (2018). Antarctica's ecological isolation will be broken by storm-driven dispersal and warming. *Nature Climate Change*, *8*, 704–708. https://doi.org/10.1038/s41558-018-0209-7

Froyland, G., Stuart, R. M., & van Sebille, E. (2014). How well-connected is the surface of the global ocean?. *Chaos*, *24*(3), 033126. https://doi.org/10.1063/1.4892530

Haller, G., & Sapsis, T. (2008). Where do inertial particles go in fluid flows? *Physica D: Nonlinear Phenomena*, *237*(5), 573–583. https://doi.org/10.1016/j.physd.2007.09.027

Hardesty, B. D., Harari, J., Isobe, A., Lebreton, L., Maximenko, N., Potemra, J., et al. (2017). Using numerical model simulations to improve the understanding of micro-plastic distribution and pathways in the marine environment. *Frontiers in Marine Science*, *4*, 30. https://doi.org/10.3389/fmars.2017.00030

Isobe, A., Uchiyama-Matsumoto, K., Uchida, K., & Tokai, T. (2017). Microplastics in the Southern Ocean. *Marine Pollution Bulletin*, *114*(1), 623–626. https://doi.org/10.1016/j.marpolbul.2016.09.037

Jambeck, J. R., Geyer, R., Wilcox, C., Siegler, T. R., Perryman, M., Andrady, A., et al. (2015). Plastic waste inputs from land into the ocean. *Science*, *347*(6223), 768–771. https://doi.org/10.1126/science.1260352

Kaiser, D., Kowalski, N., & Waniek, J. J. (2017). Effects of biofouling on the sinking behavior of microplastics. *Environmental Research Letters*, *12*(12), 124003. https://doi.org/10.1088/1748-9326/aa8e8b

Kooi, M., Reisser, J., Slat, B., Ferrari, F. F., Schmid, M. S., Cunsolo, S., et al. (2016). The effect of particle properties on the depth profile of buoyant plastics in the ocean. *Scientific Reports*, *6*(1), 33882. https://doi.org/10.1038/srep33882

Kooi, M., Van Nes, E. H., Scheffer, M., & Koelmans, A. A. (2017). Ups and downs in the ocean: Effects of biofouling on vertical transport of microplastics. *Environmental Science and Technology*, *51*(14), 7963–7971. https://doi.org/10.1021/acs.est.6b04702

Kubota, M. (1994). A mechanism for the accumulation of floating marine debris north of Hawaii. *Journal of Physical Oceanography*, *24*(5), 1059–1064. https://doi.org/10.1175/1520-0485(1994)024<1059:AMFTAO>2.0.CO;2

Kubota, M., Takayama, K., & Namimoto, D. (2005). Pleading for the use of biodegradable polymers in favor of marine environments and to avoid an asbestos-like problem for the future. *Applied Microbiology and Biotechnology*, *67*(4), 469–476. https://doi.org/10.1007/s00253-004-1857-2

Kukulka, T., & Brunner, K. (2015). Passive buoyant tracers in the ocean surface boundary layer: 1. Influence of equilibrium wind-waves on vertical distributions. *Journal of Geophysical Research: Oceans*, *120*, 3837–3858. https://doi.org/10.1002/2014JC010487

Kukulka, T., Proskurowski, G., Morét-Ferguson, S., Meyer, D. W., & Law, K. L. (2012). The effect of wind mixing on the vertical distribution of buoyant plastic debris. *Geophysical Research Letters*, *39*, L07601. https://doi.org/10.1029/2012GL051116

Lange, M., & van Sebille, E. (2017). Parcels v0.9: Prototyping a Lagrangian ocean analysis framework for the petascale age. *Geoscientific Model Development*, *10*(11), 4175–4186. https://doi.org/10.5194/gmd-10-4175-2017

Lebreton, L., Greer, S. D., & Borrero, J. C. (2012). Numerical modelling of floating debris in the world's oceans. *Marine Pollution Bulletin*, *64*(3), 653–661. https://doi.org/10.1016/j.marpolbul.2011.10.027

Lebreton, L., Slat, B., Ferrari, F., Sainte-Rose, B., Aitken, J., Marthouse, R., et al. (2018). Evidence that the Great Pacific Garbage Patch is rapidly accumulating plastic. *Scientific Reports*, *8*(1), 4666. https://doi.org/10.1038/s41598-018-22939-w

Lebreton, L., Van Der Zwet, J., Damsteeg, J. W., Slat, B., Andrady, A., & Reisser, J. (2017). River plastic emissions to the world's oceans. *Nature Communications*, *8*, 15611. https://doi.org/10.1038/ncomms15611

Lusher, A. L., Tirelli, V., O'Connor, I., & Officer, R. (2015). Microplastics in Arctic polar waters: The first reported values of particles in surface and sub-surface samples. *Scientific Reports*, *5*, 14947. https://doi.org/10.1038/srep14947

Madec, G. (2008). *NEMO ocean engine*. France: Note du Pôle de modélisation.

Madec, G., & Imbard, M. (1996). A global ocean mesh to overcome the North Pole singularity. *Climate Dynamics*, *12*(6), 381–388. https://doi.org/10.1007/BF00211684

Maximenko, N., Hafner, J., & Niiler, P. (2012). Pathways of marine debris derived from trajectories of Lagrangian drifters. *Marine Pollution Bulletin*, *65*(1-3), 51–62. https://doi.org/10.1016/j.marpolbul.2011.04.016

Niiler, P. P., & Paduan, J. D. (1995). Wind-driven motions in the northeast Pacific as measured by Lagrangian drifters. *Journal of Physical Oceanography*, *25*(11), 2819–2830. https://doi.org/10.1175/1520-0485(1995)025<2819:WDMITN>2.0.CO;2

Obbard, R. W., Sadri, S., Wong, Y. Q., Khitun, A. A., Baker, I., & Thompson, R. C. (2014). Global warming releases microplastic legacy frozen in Arctic Sea ice. *Earth's Future*, *2*(6), 315–320. https://doi.org/10.1002/2014EF000240

Peeken, I., Primpke, S., Beyer, B., Gütermann, J., Katlein, C., Krumpen, T., et al. (2018). Arctic sea ice is an important temporal sink and means of transport for microplastic. *Nature Communications*, *9*(1), 1505. https://doi.org/10.1038/s41467-018-03825-5

Reisser, J., Slat, B., Noble, K., Du Plessis, K., Epp, M., Proietti, M., et al. (2015). The vertical distribution of buoyant plastics at sea: An observational study in the North Atlantic Gyre. *Biogeosciences*, *12*(4), 1249–1256. https://doi.org/10.5194/bg-12-1249-2015

Ryan, P. G. (2015). Does size and buoyancy affect the long-distance transport of floating debris?. *Environmental Research Letters*, *10*(8), 84019. https://doi.org/10.1088/1748-9326/10/8/084019

van Sebille, E., England, M. H., & Froyland, G. (2012). Origin, dynamics and evolution of ocean garbage patches from observed surface drifters. *Environmental Research Letters*, *7*(4), 44040. https://doi.org/10.1088/1748-9326/7/4/044040

van Sebille, E., Wilcox, C., Lebreton, L., Maximenko, N., Hardesty, B. D., Van Franeker, J. A., et al. (2015). A global inventory of small floating plastic debris. *Environmental Research Letters*, *10*(12), 124006. https://doi.org/10.1088/1748-9326/10/12/124006

Waller, C. L., Griffiths, H. J., Waluda, C. M., Thorpe, S. E., Loaiza, I., Moreno, B., et al. (2017). Microplastics in the Antarctic marine system: An emerging area of research. *Science of the Total Environment*, *598*, 220–227. https://doi.org/10.1016/j.scitotenv.2017.03.283

Woodall, L. C., Sanchez-Vidal, A., Canals, M., Paterson, G. L. J., Coppock, R., Sleight, V., et al. (2014). The deep sea is a major sink for microplastic debris. *Royal Society Open Science*, *1*(4), 14,0317–14,0317. https://doi.org/10.1098/rsos.140317

Ye, S., & Andrady, A. L. (1991). Fouling of floating plastic debris under Biscayne Bay exposure conditions. *Marine Pollution Bulletin*, *22*(12), 608–613. https://doi.org/10.1016/0025-326X(91)90249-R